Ab initio study of curvature effects on the physical properties of the Xe-doped nanotubes and nanoropes

2005 J. Phys.: Condens. Matter 17 2085

(http://iopscience.iop.org/0953-8984/17/13/008)

INSTITUTE OF PHYSICS PUBLISHING JOURNAL OF PHYSICS: CONDENSED MATTER

J. Phys.: Condens. Matter **17** (2005) 2085–2110 doi:10.1088/0953-8984/17/13/008

Ab initio study of curvature effects on the physical properties of the Xe-doped nanotubes and nanoropes

B K Agrawal, S Agrawal and S Singh

Physics Department, Allahabad University, Allahabad, 211002, India

Received 18 October 2004, in final form 17 February 2005
Published 18 March 2005
Online at stacks.iop.org/JPhysCM/17/2085

Abstract

A systematic comprehensive *ab initio* investigation of the energetics, structural, electronic, and optical properties of weakly and heavily Xe-doped ultrathin 4 Å and large-diameter carbon nanotubes has been performed. The contributions of the dispersion as well as the zero-point energies have been considered. The effects of the tube diameter and the different chiralities of the carbon nanotubes on the adsorbant-induced physical properties have been investigated. The favoured tubes for Xe atom adsorption are armchair (n, n) tubes, and one may not observe any appreciable surface Xe adsorption on zigzag $(n, 0)$ or chiral (m, n) tubes. The band gap of a semiconducting achiral zigzag nanotube is reduced whereas the band gap of a chiral semiconducting tube is enhanced by the adsorption of Xe atoms. Xe adsorption in/on the metallic tubes creates extra (one or more) conductive channels which run inside/outside the nanotubes and may result in quite enhanced conduction. The optical absorption of the achiral (chiral) 4 Å diameter tube is considerably changed (unchanged) by the adsorption of the Xe atoms. The calculated peaks in large-diameter pristine nanotubes have been detected in the experimental measurements. In the (10, 0) and (10, 10) nanotubes, the small adsorption of Xe does not change the optical absorption of the pristine tube. The computed binding energy and the saturation Xe concentration are in reasonable agreement with the experimental data available for the (10, 10) nanotube.

1. Introduction

The unique nanopore structures and the reactivity of single-walled carbon nanotubes (SWCNTs) make them accessible to physisorption or chemisorption of atoms or molecules. The absorption significantly affects various physical properties of the SWCNTs, such as the structural, electronic, thermal and optical ones. The adsorption by the SWCNTs causes very fascinating and important applications, including gas storage (Schlapbach and Zuttel 2001, Hirscher *et al* 2002), electronic and thermal properties (Kong *et al* 2000, Collins *et al* 2000, Sumanasekera *et al* 2000), field emission (Saito *et al* 2002), biotechnology (Shim *et al* 2002),

catalysis, differential absorption, and nanowire and nanotube production (Tsang *et al* 1994, Ajayan *et al* 1993). The SWCNTs can also serve as templates to fabricate reproducibly very thin wires and tubes within controllable sizes. These products can be employed in practice as conducting connects in nanodevices based on molecular electronics. The guest atoms or molecules may be adsorbed either inside the SWCNTs or on the surfaces or at the grooves or the interstitial channels of the bundles of SWCNTs.

The phenomenon of gas adsorption may be studied by some experimental techniques such as adsorption measurements (Mackie *et al* 1997, Weber *et al* 2000, Talapatra *et al* 2000) and NMR (Kleinhammes *et al* 2003), which have been performed on the various inert atoms or molecules like Xe, CH_4, C_2H_6, and Ne. The adsorption of Xe atoms have been investigated experimentally by two groups of workers, (Weber *et al* 2000, Talapatra *et al* 2000, Zambano *et al* 2001, Kuznetsova *et al* 2000, Simonyan *et al* 2001). Saturated Xe coverage and the binding energy have been measured by them.

A number of theoretical calculations at different levels have been performed on the adsorption of molecules (Giannozzi *et al* 2002, Zhao *et al* 2002, Akai and Saito 2003, Dag *et al* 2003, Durgun *et al* 2003) and atoms (Dresslhaus *et al* 1999, Stan *et al* 2000, Shi and Johnson 2003, Siber 2003). In these phenomenological or simulation calculations, a summation of the two-body interactions of Lennard-Jones type were considered to calculate the system energies of the wide tubes. No *ab initio* calculation for the adsorption of Xe atoms on small- and large-diameter nanotubes and ropes is available, to the knowledge of the authors.

The theoretical study of the adsorption of atoms inside or outside the nanotubes is essential for understanding the various types of processes and functions, such as: (i) What are the geometries and the types of bonding between the adsorbed atom and the nanotube? (ii) How are the physical properties of the nanotubes affected by the adsorption of atoms? (iii) How do the altered physical properties depend upon the different diameters and chiralities of the nanotubes? In the present study, we address all these questions.

In the present investigation, we make a first-principles study of the adsorption of Xe atoms on the various sites of small-diameter 4 Å SWCNTs and some important ropes, and also on large-diameter nanotubes of different chiralities. The effects of the curvature of the nanotubes on the adsorption of Xe atoms are also investigated. A fully self-consistent pseudopotential method using density functional theory (DFT) in the generalized gradient approximation (GGA) as well as in the local density approximation (LDA) has been adopted. The contributions of the dispersion as well as the zero-point energies have been considered.

2. Method and technical details

The calculations have been performed in a self-consistent manner using the ABINIT[1] code, which uses pseudopotential and plane waves along with the density functional theory. An efficient fast Fourier transform algorithm (Goedecker 1997) is used for the conversion of the wavefunctions between the real and reciprocal lattices. The wavefunctions are determined in a fixed potential according to a state by state or band by band conjugate gradient algorithm (Payne 1992, Gonze 1996). The self-consistent potential is determined by using a potential-based conjugate gradient algorithm. We consider a soft non-local pseudopotential of Troullier and Martins (1991) within a separable approximation (Kleinman and Bylander 1982) and use the exchange correlation potential of Perdew *et al* (1996) in the GGA which is generated by FHI code (Fuchs and Scheffler 1999). The above method has been successfully applied for

[1] ABINIT code is a common project of the Université catholique de Louvain, Corning Incorporated and other contributors.

the study of small-diameter 4 Å (3, 3) and comparatively large-diameter (6, 6) nanotubes and their ropes by the present authors (Agrawal *et al* 2003, 2004).

All the Xe-CNT structures have been optimized to achieve minimum energy by relaxing both the lattice constants and the atomic positions in the unit cell simultaneously. It may be pointed out that the binding energy depends upon the number of the chosen k-points in the Brillouin zone (BZ) as well as on the plane wave cut-off energy, and one should obtain convergence with respect to both these parameters, a necessary requirement which has been overlooked in earlier publications. The present results for the Xe-doped tubes have been obtained after achieving convergence w.r.t. to both the number of k-points and the cut-off energy.

The number of atoms in an unit cell of the isolated (3, 3), (5, 0), (4, 2), (10, 0) and (10, 10) nanotubes is 12, 20, 56, 40 and 40, respectively. In the nanoropes, this number of atoms is doubled or tripled for groove or interstitial sites, respectively.

In general, the studied Xe-CNT configurations have been optimized for Hellmann–Feynman forces as small as 10^{-2} eV Å^{-1} on each atom except in some cases where the forces are higher but less than 10^{-1} eV Å^{-1}. Sufficient vacuum space has been chosen around nanotubes adsorbed with Xe atoms to avoid interference effects between the neighbouring isolated nanotubes in supercell geometries. In all cases, the minimum separation between the Xe atom of one doped tube and the neighbouring doped nanotube was more than 10 Å. The cut-off energy for the plane wave basis was varied from 40 to 90 Ryd for the optimization. To achieve convergence, a cut-off energy of 40 Ryd has been seen to be sufficient in the small-diameter 4 Å tubes but a large value of 80 Ryd is necessary in the large-diameter tubes.

3. Calculation and results

3.1. Structural properties

For establishing the stability of a configuration, we define a chemical binding energy (CBE) of the system by subtracting the optimized energy of the unit cell of the doped nanotube from the sum of the optimized energies of the unit cell of the undoped nanotube and that of the unit cell of the isolated chain of the Xe atoms (taken from the doped tube) and divide the difference by the number of Xe atoms in the unit cell. The CBE is thus the gain in energy of the configuration per Xe atom. It may be noted that the Xe atoms per unit cell give rise to infinitely extended straight chains of Xe atoms parallel to the tube axis inside or outside it. The nanotube thus works as template for the creation of linear/zigzag chains inside the tube or circular tubes of Xe atoms around the tube.

It is known that the DFT theory both in GGA and LDA takes into account only the short range interactions, namely the chemical ones, and we call this calculated binding energy the chemical binding energy (CBE) here. DFT does not include the weak long range van der Waals (vdW) interactions or the dispersion forces. In the case of chemisorption of active atoms or molecules, strong chemical binding exists, and the small contribution of the vdW energy is often omitted. However, in the case of the physisorption of saturated or inert atoms or molecules such as Xe atoms, the contributions of both the short range and long range vdW interactions are comparable, and in some cases the latter dominates and thus one has to consider both contributions. For the physisorption of inert Xe atoms on carbon nanotubes, we include the attractive vdW interaction energy here by employing the relation

$$E_{\mathrm{vdW}} = -\sum_i \sum_j C_{ij} \left(\frac{1}{r_{ij}}\right)^6 \tag{1}$$

where C_{ij} is a parameter having units of energy $\times$ distance^6, and the subscripts i, j stand for the Xe and C atoms, respectively.

For the determination of C_{ij} for the Xe-CNT vdW interaction, we employ the values of C_{ij} for the atoms given by Halgren (1992) and use the combination relation within the Slater–Kirkwood approximation. The value of C_{ij} is obtained as equal to 2001.7 eV au^6. In determining the vdW energy, we have checked the convergence of the calculated vdW energy by including more and more C atoms of the infinitely long carbon tube.

In a reliable quantitative estimation of the BE, another parameter which needs to be considered is the zero-point vibrational energy (ZP), given by

$$E_{\mathrm{zp}} = \tfrac{1}{2} \sum_i \hbar\omega_i \tag{2}$$

where the sum is over all the phonon frequencies (ω_i) for all atoms in an unit cell.

For the estimation of E_{zp}, a quite sophisticated calculation for the phonon dispersion curves and the density of phonon states has to be performed, which is beyond the scope of the present study. We use a simple method for the estimation of E_{zp}. We study the motion of the adsorbed Xe atom lying above the centre of the hexagon formed by the C atoms, keeping the carbons stationary for each Xe-tube configuration within an *ab initio* pseudopotential theory. We calculate the phonon energies at two symmetric points of the BZ, the point ($q = 0, 0, 0$) lying at the centre of the BZ and another at the boundary of BZ, ($q = 0, 0, 0.5$).

One Xe atom in the unit cell will produce in all three modes, one longitudinal mode, having motion along the tube axis, and two transverse modes normal to the tube axis. The frequencies of the three modes have been computed, and as they vary, the averaged values for the three modes have been taken for the determination of E_{zp}. This zero-point energy is then subtracted from the sum of the chemical binding energy and the vdW energy.

We have considered all the various stable configurations of the nanotube with one or more than one Xe atom per unit cell both inside and outside the tubes, separately. The number of Xe atoms saturating the intake of the Xe atoms depends on the particular tube. A Xe atom lying on the axis of the tube does not change the point-group symmetry of the host. However, a Xe atom lying on the surface of the tube changes the point-group symmetry of the host tube. On the surface of the tubes, the studied sites are above the centre of the hexagon formed by six host C atoms (mid-hexagon), the Xe atom residing either above the mid-point of the C–C bond (mid-bond) or at the top of a C atom of the host tube (top). As a typical case, we depict a (4, 2) nanotube doped with 1-Xe atom lying on the surface of the tube in a plane normal to tube axis in figure 1. Here all the atoms have been projected in one plane.

We have performed calculations for a Xe atom per unit cell residing in a groove formed by the two surfaces of the nanotubes of a nanorope containing three parallel 4 Å diameter tubes. The calculated BE turns out to be negative and of high magnitude, which leads either to instability or an adsorption of a very low concentration of Xe atoms.

Similarly, our calculation for a Xe atom present on an interstitial site of a rope formed by three nearest-neighbouring small- or large-diameter nanotubes gives a negative BE of large magnitude, and rules out the possibility of the insertion of Xe atoms between the nanotubes in a bundle. The presence of a Xe atom inside a large-diameter tube like a (10, 0) or (10, 10) tube is, however, favoured.

3.1.1. Small-diameter nanotubes. We first investigate the three types of the smallest-diameter 4 Å diameter nanotubes, two achiral (the armchair (3, 3) and the zigzag (5, 0)) and one chiral (4, 2), and study the chirality-dependent properties. The diameters of the undoped (5, 0), (3, 3) and (4, 2) nanotubes are 4.10, 4.34 and 4.28 Å, respectively. We extend our study to the

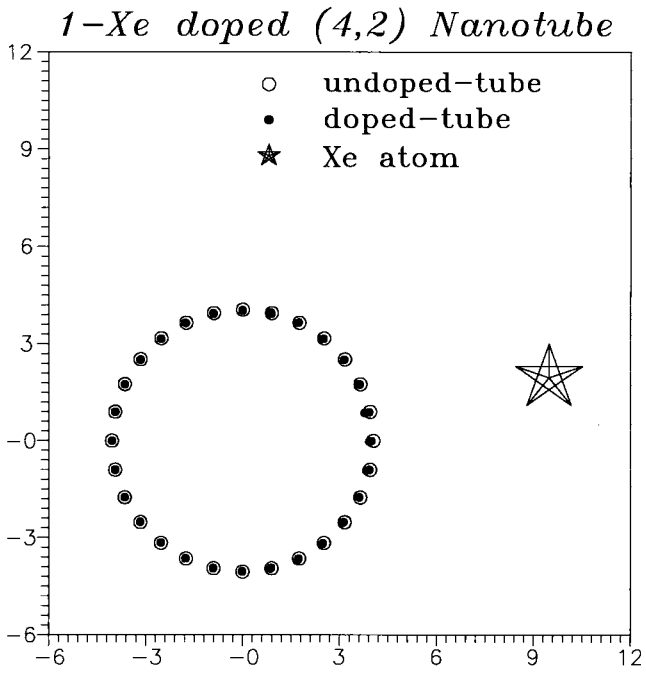

Figure 1. Atomic configuration of an optimized (4, 2) nanotube containing 1-Xe atom on the surface of the tube. All the atoms have been projected in one plane.

larger-diameter nanotubes like (10, 0) and (10, 10) which have been realized in practice to see the role of the large diameter of the tube on the adsorption. The diameters of the zigzag (10, 0) and the armchair (10, 10) nanotubes are 7.85 and 13.5 Å, respectively.

As the size of the Xe atom is comparatively large for the small-diameter 4 Å nanotube, its insertion inside any of the small-diameter 4 Å nanotubes is not favoured, as such configurations are found to be unstable.

We find that the nanotubes are slightly or highly buckled, i.e., they reveal radial deformation all along the length. This radial deformation is measured by the percentage of the difference between the maximum and minimum radii of the tube with respect to the averaged radius of the tube, and is named buckling.

Convergence of chemical binding energy. First, we obtain the values of the CBE in LDA and GGA and investigate its variation w.r.t. to the different functionals for exchange and correlation as in Perdew *et al* (1996), where it is named PBE, and in Becke (1988) and Lee *et al* (1988), where it is named BLYP. The CBEs for one k-point for the adsorption of Xe atoms on the (5, 0) nanotube in the above three approximations are shown in table 1. One observes a positive value of CBE for Xe in the LDA against a negative value in the GGA, which points towards the overbinding of Xe as has been observed in other cases, such as the adsorption of O_2 on nanotubes (Zhao *et al* 2002, Dag *et al* 2003). We thus make future calculations only in the GGA.

Further, we observe that in the GGA, the CBE obtained for the BLYP exchange and correlation functional is quite small as compared to the PBE functional, which does not seem to be realistic as it will lead to quite low values of the binding energies contrary to the experimentally observed values in the large-diameter (10, 10) tubes. We thus choose the PBE exchange and correlation functional for obtaining our final values for the CBEs.

Table 1. Chemical binding energy (CBE) in eV in LDA and GGA with different exchange–correlation functionals for the adsorption of 1-Xe atom on the surface of the (5, 0) carbon nanotube for a cut-off energy of 80 Ryd.

		GGA	
Position of Xe atom	LDA	PBE	BLYP
1-Xe			
Surface			
Mid-hexagon	0.100	−0.038	−0.161

Table 2. Variation of chemical binding energy (CBE) in eV with respect to k-points for one Xe-doped (3, 3) and (5, 0) carbon nanotubes for a cut-off energy of 80 Ryd.

k-points	(3, 3) nanotube	(5, 0) nanotube
1		−0.038
2		−0.041
6	0.343	−0.038
8	0.350	

Table 3. Variation of chemical binding energy (CBE) in eV with cut-off energy for one Xe-doped (3, 3), (5, 0), (10, 10) and (10, 0) carbon nanotubes.

Cut-off energy	Small-diameter tubes		Large-diameter tubes	
(Ryd)	(3, 3) (6-$k$pts)	(5, 0) (2-$k$pts)	(10, 0) (2-$k$pts)	(10, 10) (6-$k$pts)
40	0.337	−0.044	−0.686	−0.463
60	0.343	−0.038		
80	0.337	−0.041	−0.046	0.180
90	0.343	−0.041	−0.046	0.180

Xe-doped (3, 3) nanotube

1-Xe. At first, the convergence of CBE with the number of k-points in the BZ was tested. We observe that the CBE converges within 2% with increase in the number of k-points in BZ. As an example, the values of CBE obtained for six and eight k-points in the BZ for the surface adsorption of Xe atoms on the (3, 3) tube are depicted in table 2. It may be noted here that the stability of the Xe-CNT system is not seen if one choses a smaller number of k-points.

We then investigate the convergence of the CBE with the cut-off energy of the plane waves. We varied the cut-off energy from 40 to 90 Ryd and observed that the CBE converged within 2% for such a large cut-off energy variation. The actual values of computed CBEs for several cut-off energies for the adsorption of Xe on the (3, 3) tube is shown in table 3.

The calculated phonon energies for one Xe-doped (3, 3) nanotube at the $q = 0, 0, 0$ and $0, 0, 0.5$ points are 16.4, 14.9, 0.0 meV and 19.5, 17.7, 56.3 meV, respectively. The displacement of the frequencies for each q-point correspond to Xe motion along (x, y, z) directions. The zero-point contribution turns out to be 31.2 meV.

The final BEs (CBE + the vdW energy − the zero-point energy) for the various locations of the Xe atoms lying on the surface of the (3, 3) nanotube, the averaged tube diameter, the averaged minimum separation between the host C atom and the adsorbed Xe atom and tube buckling are shown in table 4.

The BEs for the two most favourable mid-hexagonal and mid-bond sites are positive and quite appreciable (table 4). The final BEs for the mid-hexagonal and mid-bond sites are 0.672

Table 4. Total binding energy (BE) per Xe atom in eV for the various concentrations of adsorption of Xe atoms on (3, 3) nanotubes. The final energy is equal to (CBE + the van der Waals energy − the zero-point energy (=0.031 eV)). The averaged diameters of the tubes, the separation between Xe and the nearest C of the SWNT in Å and the bucklings are also included.

Positions of Xe atom	CBE	vdW energy	Final BE	Tube diameter	Xe–C distance	Buckling (%)
1-Xe Surface						
Mid-hexagon	0.482	0.221	0.672	4.20	3.38	1.1
Mid-bond (normal to z-axis)	0.337	0.194	0.500	4.21	3.24	0.9
3-Xe Surface						
Mid-hexagon	0.174	0.225	0.368	4.20	3.37	1.0
1-Xe Groove-site	Unstable					
1-Xe Interstitial between 3 tubes	Unstable					

and 0.500 eV, respectively. Here, the studied mid-bond site is the one where the Xe is residing above the middle of that C–C bond which is normal to the tube axis. In fact, the binding of the Xe residing on the mid-bond site of the other C–C bond which is nearly parallel to the tube axis is seen to be weaker. This is an expected behaviour because the C–C bonds which are normal to the tube axis are the maximum curved ones and thus the most strained ones on the formation of the tube.

The lattice constant for the (3, 3) tube along the tube axis is 2.39 Å. We have determined the equilibrium separation between the two Xe atoms kept in vacuum as equal to 4.83 Å, and obtain no binding, i.e., CBE = 0.0 eV. As the present separation of 2.39 Å between the two Xe atoms along the chain formed along the tube axis is smaller than the equilibrium separation of 4.83 Å between the two Xe atoms in isolation, there is significant repulsive Xe–Xe interaction contribution to the energy of the doped tube.

It may be pointed out that the isolated minimum energy Xe linear chain is unstable as it has negative chemical binding energy. The Xe chain is stabilized by the underneath carbon nanotube.

3-Xe. A maximum adsorbant concentration is obtained by placing three Xe atoms lying in a plane normal to the tube axis on the mid-hexagonal sites on the surface of the tube. For this configuration, the final BE decreases from 0.672 to 0.368 eV. The Xe–C distance for this configuration remains essentially the same as for the one Xe case and the induced buckling also remains practically unaltered. This configuration of 3-Xe atoms forms a circular tube of Xe atoms around the (3, 3) tube. One Xe atom per unit cell corresponds to an adsorbant concentration of 8.3%. We thus expect a maximum adsorption of about 25% of Xe atoms with respect to the number of host C atoms.

A perusal of table 4 reveals that the contraction in the averaged diameter of the (3, 3) tube induced by the Xe atoms is about 3%. The variation in the minimum separation between the C atom of the host tube and the Xe atom lies within 5%. The buckling induced by the Xe atoms is quite small and is about 1.0%.

Table 5. Total binding energies (BE) per Xe atom in eV for the various concentrations of adsorption of Xe atoms on (5, 0) nanotubes. The final energy is equal to (BE + the van der Waals energy − the zero-point energy (=0.022 eV)). The averaged diameters of the tubes, the separation between Xe and the nearest C of the SWNT in Å and the bucklings are also included.

Positions of Xe atom	CBE	vdW energy	Final BE	Tube diameter	Xe–C distance	Buckling (%)
1-Xe Surface						
Mid-hexagon	−0.041	0.141	0.078	4.07	3.70	11.4
Top	−0.103	0.168	0.043	4.05	3.27	2.5
5-Xe Surface						
Mid-hexagon	−0.059	0.161	0.080	4.07	3.52	11.5
1-Xe Groove-site	Unstable					
1-Xe Interstitial between 3 tubes	Unstable					

Xe-doped (5, 0) nanotube

Convergence of chemical binding energy. The CBE converges within 8% with increase in the number of k-points in the BZ. As an example, the values of CBE obtained for one, two and six k-points in the BZ for the surface adsorption of Xe atoms on the (5, 0) tube are depicted in table 2. In fact, for the (5, 0) tube, the vdW energy dominates over the small chemical binding energy. We then investigate the convergence of CBE with the cut-off energy of the plane waves. We varied the cut-off energy from 40 to 90 Ryd and observed that the CBE converged within 2% for such a large cut-off energy variation. The actual values of computed CBEs for the various cut-off energies for the adsorption of Xe on the (5, 0) tube are shown in table 3. The small CBE shows an alternation in the values with the cut-off energy but the variation lies within 8%.

The calculated phonon energies at the $q = 0, 0, 0$ and $0, 0, 0.5$ points are 18.0, 17.1, 0.0 meV and 18.2, 17.4, 17.6 meV, respectively. The zero-point contribution turns out to be 22.1 meV. It may be noted here that a low value of 17.6 eV for the longitudinal Xe vibration results from a comparatively large Xe–Xe separation in the (5, 0) tube as compared to a value of 56.3 eV seen for the (3, 3) tube.

The final BEs (CBE + the vdW energy − the zero-point energy) for the various locations of the Xe atoms lying on the surface of the (5, 0) nanotube, the averaged tube diameters, the averaged minimum separation between the host C atom and the C atom of the adsorbed Xe atoms and the tube buckling are shown in table 5.

1-Xe. The CBEs for the (5, 0) tube doped with 1-Xe atom on the surface are negative and their magnitude is small. The attractive vdW energies are high, and they compensate the CBEs and result in very weak binding of the Xe atoms to the CNT. The final BEs lie in the range 0.043–0.080 eV and one will not see eventually any adsorption of the Xe atoms on the (5, 0) tube at finite temperatures like 300 K, as will be discussed later.

The lattice constant for the (5, 0) tube along the tube axis is 4.23 Å. As the separation of 4.23 Å between the two Xe atoms along the chain is again smaller than the separation of 4.83 Å between the two Xe atoms in isolation, there is a small repulsive contribution to the energy of the doped tube because of the Xe–Xe interactions.

Table 6. Total binding energies (BE) per Xe atom in eV for the adsorption of Xe atom on (4, 2) nanotube. The final energy is equal to (BE + the van der Waals energy − the zero-point energy (=0.022 eV)). The averaged diameters of the tubes, the separation between Xe and C of the SWNT in Å and the buckling are also included.

Positions of Xe atom	CBE	vdW energy	Final BE	Tube diameter	Xe–C distance	Buckling (%)
1-Xe Surface Mid-bond	−0.079	0.149	0.048	4.27	3.47	6.1
1-Xe Groove-site	Unstable					
1-Xe Interstitial between 3 tubes	Unstable					

5-Xe. Further increase in the adsorbant concentration by placing 5-Xe atoms lying in a plane normal to the tube axis on all the mid-hexagonal sites on the surface of the tube in an unit cell around the (5, 0) tube is also not favoured, as the BE remains quite small.

A perusal of table 5 reveals that the changes in the averaged diameter of the tube induced by the Xe atoms is less than 2%. The variation in the minimum separation between the C atom of the host tube and the Xe atom lies within 12.3%. On the other hand, the buckling induced by the Xe atoms in the various nanotube configurations is large and lies within 12%.

Xe-doped (4, 2) nanotube

1-Xe. In the case of the (4, 2) nanotube (see table 6), the BE for 1-Xe atom residing on the surface mid-bond site is again negative and small, similar to the other 4 Å (5, 0) nanotube. We carry over the zero-point vibrational energy of 0.022 eV calculated earlier for the (5, 0) here. The addition of the vdW energy and the subtraction of the zero-point energy gives the final BE as 0.048 eV. The binding of a Xe atom at another site, say the top site, is slightly smaller than at the mid-bond site. As the smallest unit cell contains 56 C atoms, one Xe atom in the unit cell corresponds to a dopant concentration of about 2%. However, one will not observe any adsorption of Xe atoms on the (4, 2) nanotube.

The changes induced by the Xe atoms in the averaged diameter of the (4, 2) tube is negligible. The radial distortions (buckling) induced by the adsorbed Xe atoms is 6.1%, a value which lies in between the values of the other 4 Å nanotubes. The minimum Xe–C separation is similar to that of the other 4 Å nanotubes.

3.1.2. Large-diameter nanotubes

Xe-doped (10, 0) nanotube

Endohedral adsorption

1-Xe

Convergence of chemical binding energy. The convergence of CBE with the number of k-points has also been tested in the large-diameter (10, 0) nanotube. In table 3, we present the values of CBE for the various cut-off energies and observe that the CBE changes very

Table 7. Total binding energies (BE) per Xe atom in eV for the various concentrations of adsorption of Xe atoms in or on (10, 0) nanotubes. The final energy is equal to (BE + the van der Waals energy − the zero-point energy (=0.022 eV)). The averaged diameters of the tubes, the separation between Xe and C of the SWNT in Å and the bucklings are also included.

Positions of Xe atom	CBE	vdW energy	Final BE	Tube diameter	Xe–C distance	Buckling (%)
1-Xe Inside	−0.063	0.521	0.436	7.90	3.96	0.2
1-Xe Surface Mid-hexagon	−0.046	0.157	0.089	7.92	3.72	2.5
10-Xe Surface Mid-hexagon	−0.067	0.181	0.092	7.92	3.64	2.5
1-Xe Interstitial between 3 tubes	Unstable					

significantly with the cut-off energy. It is enhanced by 0.640 eV when one goes from a cut-off energy of 40 Ryd to one of 80 Ryd, and thereafter it remain constant.

The calculated phonon energies at the $q = 0, 0, 0$ and $0, 0, 0.5$ points are 17.9, 16.3, 0.0 meV and 18.4, 17.6, 18.3 meV, respectively. The zero-point contribution turns out to be 22.1 meV.

In a medium-diameter achiral zigzag (10, 0) nanotube as shown in table 7, the CBEs for both the endohedral and exohedral adsorption of Xe atoms are again negative and small in magnitude (−0.067 to −0.046 eV) and the Xe adsorption is not favoured. The positive vdW energies dominate and make the final BEs positive. However, the quite small total binding energies seen for the exohedral adsorption will not lead to any appreciable adsorption. A quite high value of vdW energy (0.521 eV) obtained for the endohedral adsorption makes the final binding energy equal to 0.436, which will favour this adsorption. As the unit cell of the (10, 0) tube contains 40 C atoms, one Xe atom in the unit cell corresponds to an adsorbant concentration of 2.5%.

10-Xe. We increased the adsorbant concentration by placing ten Xe atoms lying in a plane normal to the tube axis on the mid-hexagonal sites on the surface of the tube and found that the BE is quite similar to that obtained for one Xe atom. The tube diameter of the (10, 0) tube changes only by 1% after the adsorption of the Xe atoms.

The minimum separation between the C atom of the host tube and the Xe atom is comparatively large, lying in the range 3.64–3.96 Å. On the other hand, the buckling for endohedral adsorption is quite small (0.2%), but is high for exohedral absorption (=2.5%).

Xe-doped (10, 10) nanotube

Endohedral adsorption

4-Xe. For the wide achiral armchair (10, 10) nanotube, one has to shift the Xe atom towards the C atoms by about 3.2 Å away from the tube axis for obtaining a minimum energy configuration. It is noted that there is no potential barrier for the motion of the Xe atom inside the tube. This observed smoothness of the (10, 10) tube for the motion of the Xe atom will lead to rapid

transport of Xe gas along the tube, as has been observed in experiments (Skoulidas *et al* 2002) performed on the adsorption of CH_4 molecules in (10, 10) tubes.

We study the maximum endohedral adsorption by placing four Xe atoms lying in a plane normal to the tube axis at the off-axis positions and find a value of CBE equal to 0.194 eV. The vdW contribution is 0.232 eV per Xe atom, which results in a final BE value of 0.383 eV. Here, each Xe atom again lies 3.2 Å away from the axis. The Xe–Xe separation inside the tube is seen to be 4.5 Å, which is smaller than the corresponding separation of 4.83 Å seen for an isolated Xe–Xe molecule. It will incur Xe–Xe repulsive contribution to the total BE. The enhanced adsorption may lead to a saturation adsorbant concentration of 10%.

The minimum separation between the C atom of the host tube and the Xe atom is comparatively large (3.79 Å). On the other hand, there is quite small buckling of 0.6% for the endohedral adsorption.

Exohedral adsorption

Convergence of chemical binding energy. In testing the convergence of CBE with the number of k-points in the large-diameter (10, 10) nanotube as shown in table 3, we find that the arguments similar to the (10, 0) tube are valid here. We find that the CBE changes very significantly with the cut-off energy. It is enhanced by 0.643 eV when one goes from a cut-off energy of 40 Ryd to one of 80 Ryd, and thereafter it remain constant.

1-Xe. For the surface adsorption, the chemical binding is comparatively weaker and the CBEs are much reduced as compared to the values seen above for the (3, 3) tube. The final BE is 0.315 eV after including a vdW contribution of 0.178 eV and subtracting a zero-point energy of 0.043 eV.

The calculated phonon energies at the $q = 0, 0, 0$ and $0, 0, 0.5$ points are 17.0, 21.5, 0.0 meV and 14.2, 12.4, 64.8, meV, respectively. The zero-point energy contribution turns out to be 43.3 meV.

The minimum Xe–C separation is comparatively small (3.20 Å). The Xe-induced buckling is quite small, of the order of $0.4 \pm 0.2\%$.

10-Xe. The exohedral adsorbant concentration was increased by placing ten Xe atoms on all the mid-hexagonal sites on the surface of the tube, and we found that the CBE becomes negative (BE $= -0.062$ eV). The binding of ten Xe atoms is thus not favoured.

A comparison of the present results with the available experimental data is warranted. The above calculated value of BE for the exohedral adsorption, 0.315 eV, is quite near to the measured values lying in the range 0.26–0.286 eV (Talapatra *et al* 2000, Kuznetsova *et al* 2000, Simonyan *et al* 2001). Here, we have invoked a cut-off Xe–C separation of 6.1 au (3.23 Å) in the above calculation of the vdW energy. In case one does not invoke this cut-off, the vdW energy is nearly doubled and the final BE is enhanced by about 50%. In view of an inherent uncertainty in the choice of the parameters for vdW energy the results seem to be quite reasonable.

The above maximum calculated Xe concentrations of 10% and 2.5% for the endohedral and the exohedral adsorption of the (10, 10) nanotube, respectively, are higher than the measured value of 4.2%. However, the experimental results have been obtained only for a mixture of nanotubes of different diameters around the (10, 10) nanotubes (Wildoer *et al* 1998, Odom *et al* 1998). The calculated results seem to be reasonable, as various types of the tubes are present in the samples which will not show any adsorption as noted above.

Table 8. Total binding energies (BE) per Xe atom in eV for the various concentrations of adsorption of Xe atoms in or on (10, 10) nanotubes. The final energy is equal to (BE + the van der Waals energy − the zero-point energy (=0.043 eV)). The averaged diameters of the tubes, the separation between Xe and C of the SWNT in Å and the bucklings are also included.

Positions of Xe atom	CBE	vdW energy	Final BE	Tube diameter	Xe–C distance	Buckling (%)
4-Xe Inside	0.194	0.232	0.383	13.80	3.79	0.6
1-Xe Surface Mid-hexagon	0.180	0.178	0.315	13.50	3.20	0.2
10-Xe Surface Mid-hexagon	−0.062	0.178	0.073	13.50	3.20	0.2
1-Xe Interstitial between 3 tubes	Unstable					

A perusal of tables 4–8 reveals that there is no obvious correlation between the BEs either with the tube diameters or with the minimum separation between the Xe atom and that of the host tube.

Adsorption at finite temperatures. In the present study, the final BEs have been obtained at 0 K. At any finite temperature, the atomic vibrational energy will be crucial in determining the adsorption of the Xe atoms. The maximum vibrational energy per atom is $3k_BT$. At 100 K, it will amount to 26 meV, whereas at 300 K, it will become 78 meV. In case the final BE is greater than this maximum vibrational energy which has been calculated on the higher-value side, one may expect the adsorption of Xe atoms on the carbon tube.

Applying this criteria for the exohedral adsorption of Xe atoms, we observe that the BEs for the adsorption on the surfaces of the armchair (3, 3) and (10, 10) nanotubes are much larger than the vibrational energies, and Xe adsorption will be seen in the experiments. On the other hand, as the BEs for the surface adsorption on the (5, 0), (4, 2) and (10, 0) tubes are comparable with the vibrational energies at 300 K, one may not observe any adsorption in practice.

For the endohedral adsorption of Xe atoms in the (10, 0) and (10, 10) tubes, the BEs are of the order of 450 meV and one will observe adsorption of Xe atoms.

3.2. Electronic structure

The electronic structure and the DOS have been calculated for the 51, 26, 11, 16 and 11 k-points chosen along the k_z-direction in the BZ for the (3, 3), (5, 0), (4, 2) and (10, 0) and (10, 10) nanotubes, respectively, with a broadening of 0.055 eV. The Fermi level (E_F) or the highest occupied state has been chosen as the origin of energy. For the DOS, the full units are states/eV/unit cell, and for brevity in our further discussion we will write units instead of the full units.

Xe-doped (3, 3) nanotube. The electronic structure and the DOS for the pristine (3, 3) nanotubes are presented in figure 2(a). The bonding and the anti-bonding (24, 25) states cross at E_F (named as Δ_F) and the tube is metallic as expected by symmetry considerations. The DOS at E_F is 0.31 units. In figure 2(a), we have shown the highest occupied single 24th state

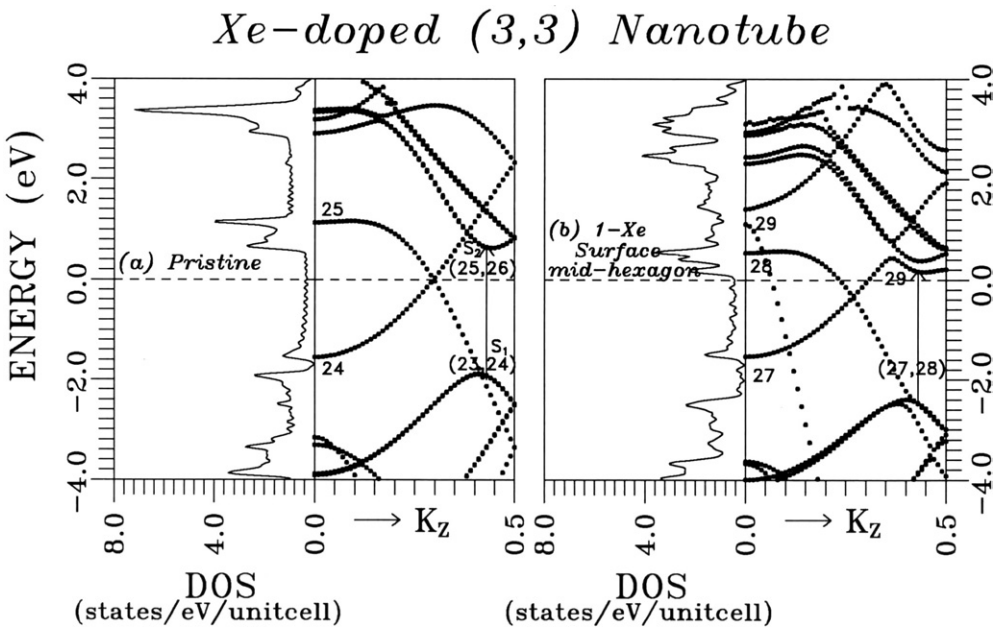

Figure 2. Electronic structure and the density of electron states in the vicinity of the Fermi level for a (3, 3) nanotube: (a) pristine, (b) 1-Xe atom on surface mid-hexagonal site. The doubly-degenerate topmost filled and the lowest unfilled states have been marked as (23, 24) and (25, 26) near the BZ boundary for the pristine tube. The numbering is different at various values of k_z. Some typical optical transitions have also been depicted.

and the lowest unoccupied single 25th state before the crossing point $k_z = 0.3$. Above the crossing point for $k_z > 0.4$, we also depict the doubly-degenerate occupied (23, 24) states and the doubly-degenerate unoccupied (25, 26) states which have come up (down) in the valence (conduction) band region with respect to the bonding–antibonding pair (24, 25) before $k_z = 0.35$. These states contain two saddle points near the boundary of the BZ in the vicinity of E_F. In fact, these states are seen to contribute to optical transitions.

1-Xe. The electronic structure and the DOS for the Xe atom residing on the surface mid-hexagonal site of a (3, 3) tube are presented in figure 2(b). These quantities are the same for the mid-bond site. The electronic structure is changed especially in the neighbourhood of E_F. This is the consequence of the breaking of the symmetry of the host tube by the Xe atom residing on the surface. The crossing of the bonding–antibonding carbon states is not disturbed but it descends below E_F. One low-lying valence state rises and cross E_F as well as the first conduction state. All the states especially lying in the neighbourhood of the BZ boundary split. At E_F, the nature of the bonding and anti-bonding states is now hybridized C(p)–Xe(p) ones. The Xe adsorption creates one more conductive channel which runs outside the nanotube. Two nearly free electron (NFE) like conduction states descend and mix with the uppermost valence state and get split. The DOS at E_F is enhanced from 0.32 units seen for the pristine tube to 0.43 units for the doped tube. The states in the vicinity of E_F have been numbered and some optical transitions have been shown for later discussion.

The electronic structure for more than one surface Xe atom is seen to be quite similar to that of the one Xe atom except that more valence states arising from the increased number of the adsorbed Xe atoms rise and cross E_F. The DOS is also enhanced.

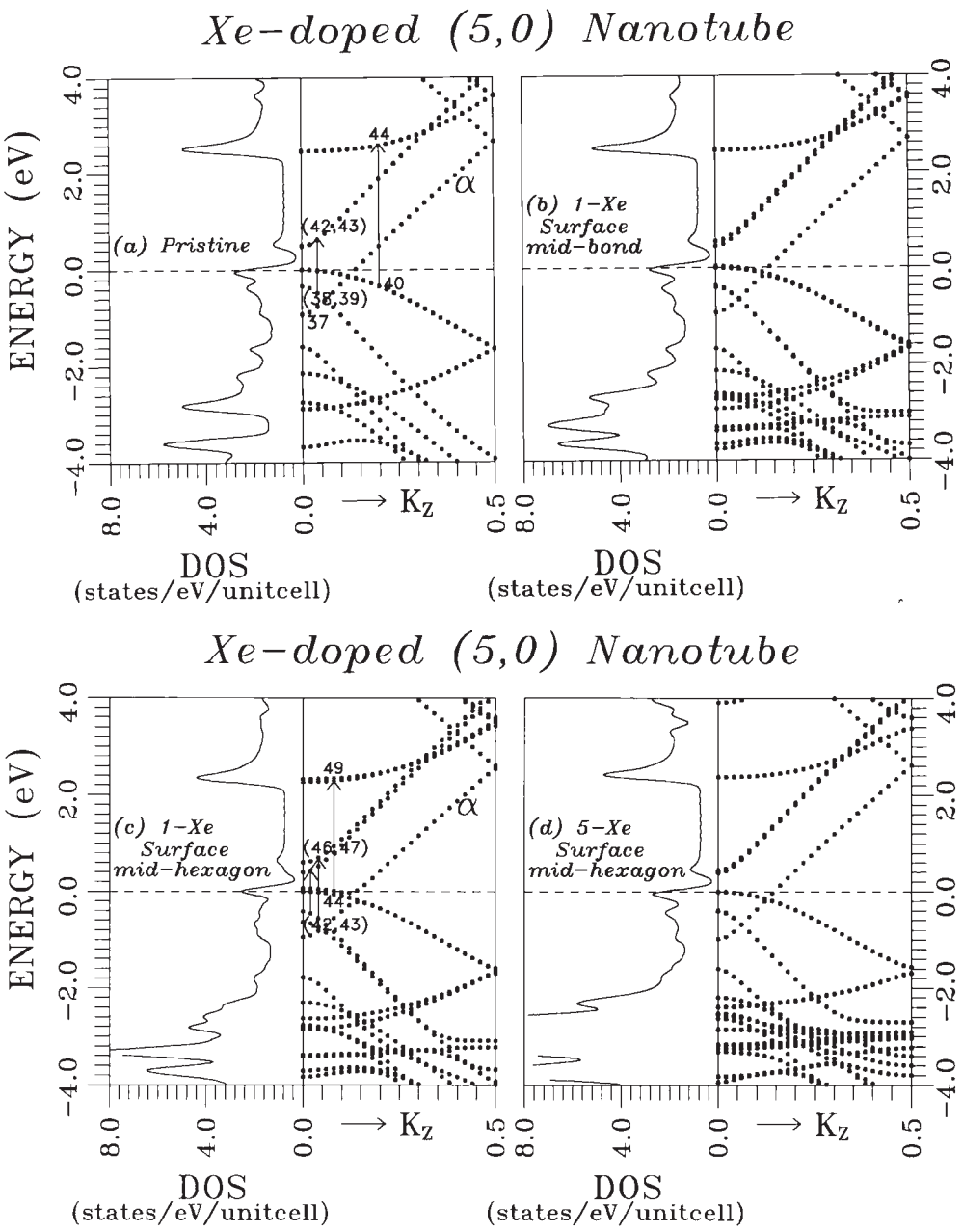

Figure 3. Electronic structure and the density of electron states in the vicinity of the Fermi level for a (5, 0) nanotube: (a) pristine, (b) 1-Xe atom on surface-mid-bond site, (c) 1-Xe atom on surface mid-hexagonal site and (d) 5-Xe atoms on surface mid-hexagonal sites. For the pristine tube, the doubly-degenerate topmost filled and the lowest unfilled states have been marked as (38–40) and (42–44) near the centre of the BZ. The numbering is different at various values of k_z. Some typical optical transitions have also been demonstrated.

Xe-doped (5, 0) nanotube. The pristine (5, 0) tube is expected to be semiconducting by symmetry considerations. However, because of the strong curvature effects, a state 'α' lying

in the conduction band region next to E_F descends quite appreciably and makes the nanotube conducting (figure 3(a)). A vHs from the valence band region occurs very near to E_F and enhances the DOS to 3.5 units. The next conduction states lies about 0.5 eV higher at $k_z = 0$. The states in the vicinity of E_F have been numbered and some optical transitions have been shown which will be discussed later.

1-Xe. The electronic structure and DOS for one Xe-doped (5, 0) nanotube for the Xe atom for the mid-bond and the mid-hexagonal sites of the surface are seen to be similar and are presented in figures 3(b) and (c), respectively. All the states especially lying in the vicinity of the E_F split. Among them, the α state and the uppermost doubly-degenerate valence state (which cross just below E_F) split. One of the split valence states rises regularly and crosses E_F. The other one bends downwards. The α state also bends, but upwards. This is the consequence of the breaking of the symmetry of the host tube by the Xe atom residing on the surface. For the mid-bond site of the Xe atom, the above splitting of states is enhanced. The DOS at E_F is 2.50 and 2.54 units for the mid-hexagonal and the mid-bond sites, respectively, which is lower than that for the pristine tube. Again, the states in the vicinity of E_F have been numbered and some optical transitions have been shown for later discussion.

5-Xe. The electronic structure and the DOS for the 5-Xe atoms residing on all the mid-hexagonal sites are shown in figure 3(d). Arguments similar to that of one Xe atom are applicable except for the enhancement in the splitting of the states. The DOS for the 5-Xe atoms at E_F is similar to that obtained for the one Xe case. One observes very high DOS in the energy range -3.0 to -4.0 eV in the valence band because of the occurrence of a large number of flat bands of the Xe states.

Xe-doped (4, 2) nanotube. The pristine (4, 2) nanotube is semiconducting, and its electronic structure and DOS are shown in figure 4(a). The electronic structure and DOS for one Xe-doped (4, 2) nanotube are presented in figure 4(b). The adsorption of Xe atoms on the surface of the (4, 2) nanotube does not cause any significant changes in the electronic structure of the pristine (4, 2) tube in the vicinity of E_F as the tube has no obvious symmetry. The valence states lying near the top of the valence band have descended. The band gap is slightly enhanced, i.e., from 0.14 to 0.19 eV, by the adsorption of 1-Xe atom.

The states in the vicinity of E_F have been numbered and some optical transitions have been shown for later discussion.

Xe-doped (10, 0) nanotubes. The pristine (10, 0) tube is semiconducting as expected by symmetry considerations (figure 5(a)). No conduction state has descended into the gap, in contrast to the situation seen earlier for the large-curvature (5, 0) nanotube. The magnitude of the semiconducting gap is 0.90 eV. Some of the states in the vicinity of E_F involved in the two lowest energy optical transitions have been numbered, and will be discussed later.

1-Xe. The electronic structure and DOS for the one Xe-doped (10, 0) nanotube for the Xe atom lying on the mid-hexagonal site of the host C-atom are presented in figure 5(b). The above quantities are quite similar for all the types of endohedral and exohedral adsorption of Xe atoms. A number of conduction states lying in the vicinity of the E_F decent towards E_F and the band gap is reduced to 0.56 eV. Again, some states in the vicinity of E_F have been numbered.

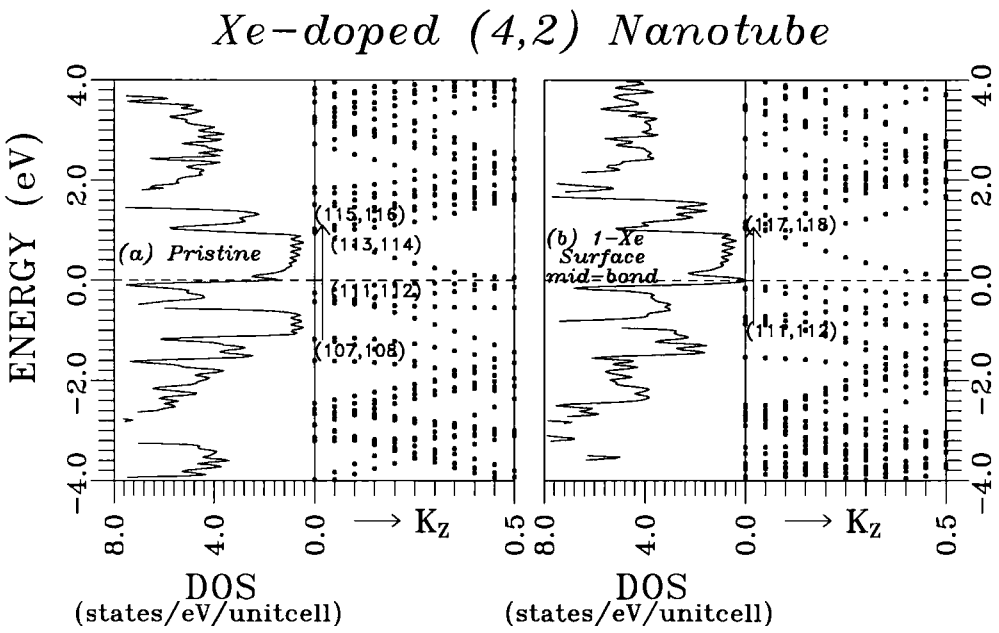

Figure 4. Electronic structure and the density of electron states in the vicinity of the Fermi level for a (4, 2) nanotube: (a) pristine, (b) 1-Xe atom on surface site. For the pristine tube, the doubly-degenerate topmost filled and the lowest unfilled states have been marked as (107–112) and (113–116) near the centre of the BZ. Some typical optical transitions have also been shown.

10-Xe. The electronic structure and DOS (figure 5(c)) for the doped (10, 0) nanotube for the adsorption of 10-Xe-on the mid-hexagonal sites of the surface are quite similar to that for the 1-Xe atom. The band gap is again equal to 0.59 eV.

Xe-doped (10, 10) nanotube. The electronic structure and the DOS for the pristine achiral armchair (10, 10) nanotube are presented in figure 6(a). The bonding and the anti-bonding (80, 81) states cross at $k_z = 0.35(\Delta_F)$ and the tube is metallic as expected by symmetry considerations. The two saddle points observed near the boundary of the BZ in the vicinity of E_F appear now for $k_z < \Delta_F$ in contrast to the (3, 3) nanotube where they were seen to lie for $k_z > \Delta_F$. In figure 6(a), we have shown the highest occupied single 80th state and the lowest unoccupied single 81st state. The DOS at E_F is seen to be 0.25 units.

1-Xe. The electronic structure and the DOS for the Xe atom residing inside and on the surface mid-hexagonal site of a (10, 10) nanotube are presented in figures 6(b) and (c), respectively. The above physical quantities are quite similar for the endohedral and the exohedral adsorptions. The electronic structure is not much changed in the neighbourhood of E_F. Although the crossing of the bonding–antibonding carbon states is not disturbed, it descends below E_F. Another low-lying valence state rises and crosses E_F similar to the (3, 3) tube and creates one more conductive channel which runs outside the nanotube. At E_F, the nature of the bonding and anti-bonding states are now the hybridized C(p)–Xe(p) ones. The states both in the conduction and valence bands quite split and give rise to more strong peaks in the DOS. The DOS is enhanced from the 0.25 units seen for the pristine tube to about 1.65 units for the surface site adsorption. Some states in the vicinity of E_F have been numbered.

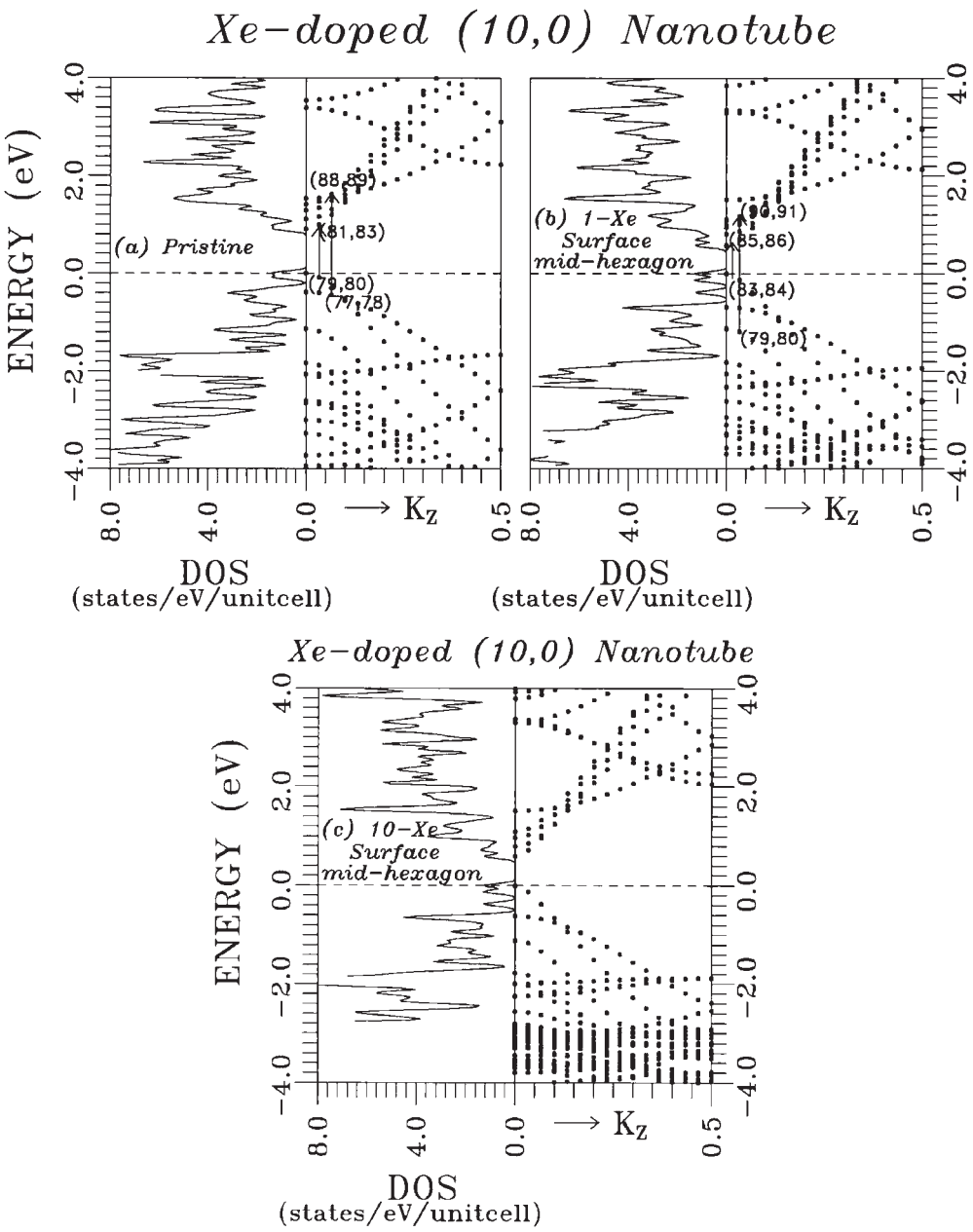

Figure 5. Electronic structure and the density of electron states in the vicinity of the Fermi level for a (10, 0) nanotube: (a) pristine, (b) 1-Xe atom on surface mid-hexagonal site, (c) 10-Xe atoms on surface mid-hexagonal sites. The doubly-degenerate topmost filled and the lowest unfilled states have been marked as (77, 78) and (81, 82) near the centre of the BZ for the pristine tube. Some typical optical transitions have also been shown.

10-Xe. The electronic structure and the DOS for 10-Xe surface atoms shown in figure 6(d) is quite similar to that of the 1-Xe adsorption. A larger number of Xe atom induced-valence states cross E_F and some conduction states also decent and cross E_F. All these extra states

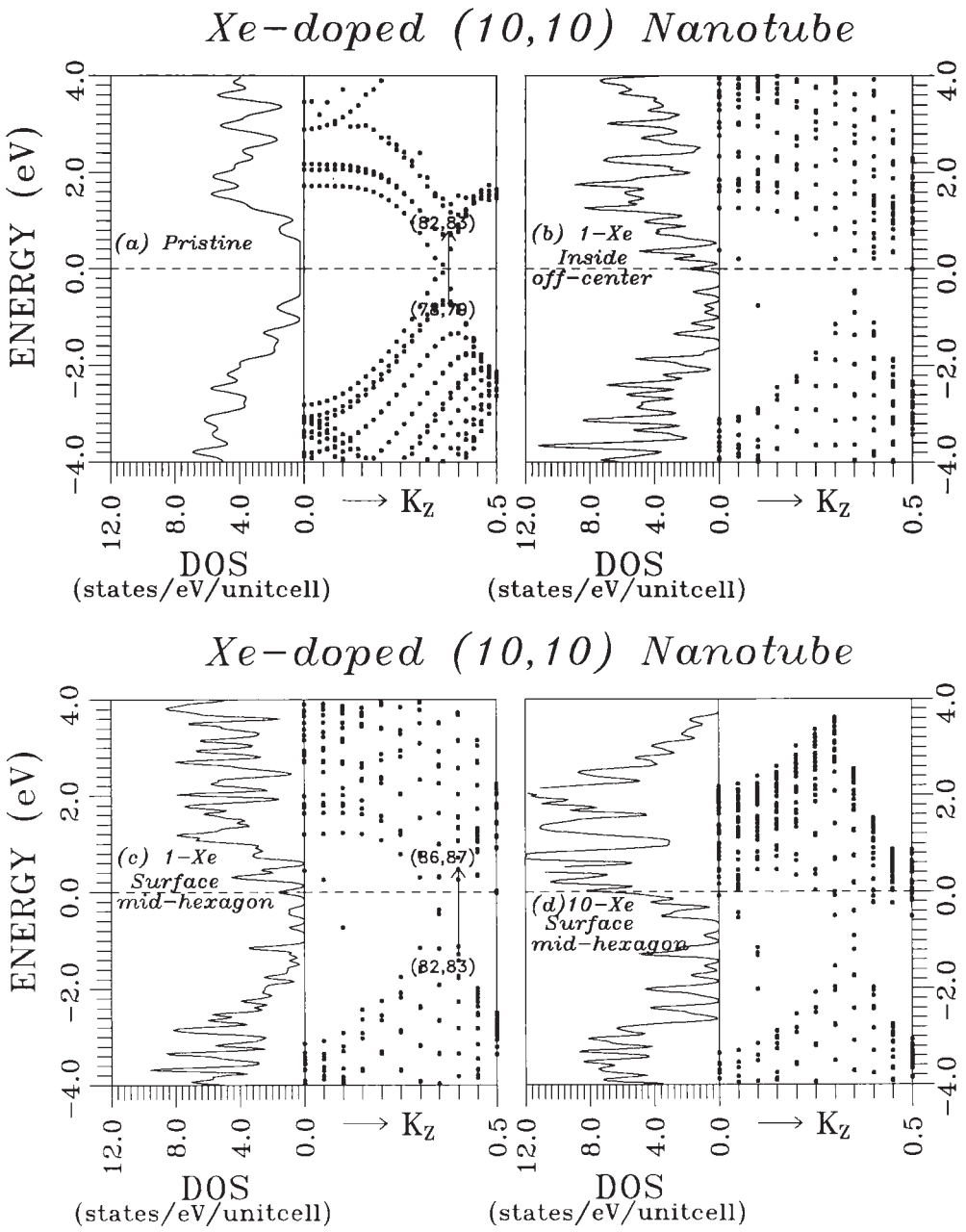

Figure 6. Electronic structure and the density of electron states in the vicinity of the Fermi level for a (10, 10) nanotube: (a) pristine, (b) 1-Xe atom inside at off-centre site, (c) 1-Xe atom on the surface mid-hexagonal site, (d) 10-Xe atoms on surface mid-hexagonal sites. For the pristine tube, the doubly-degenerate topmost filled and the lowest unfilled states have been marked as (78, 79) and (82, 83) near the boundary of the BZ. Some typical optical transitions have also been drawn.

create more conductive channels along the tube axis. The DOS is enhanced to a very high value of 7.43 units.

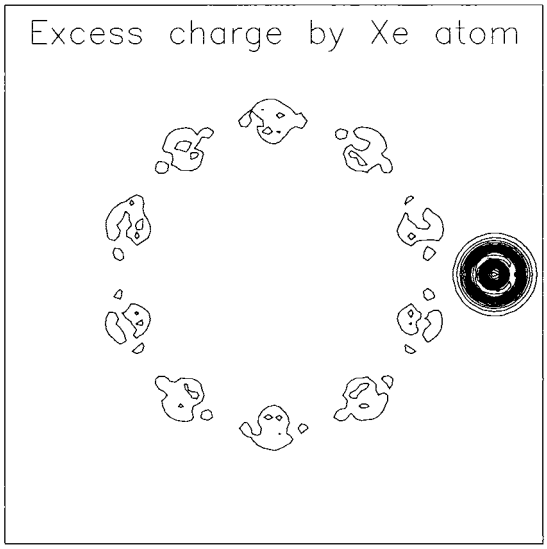

Figure 7. The excess charge of the Xe-doped tube over the pristine tube. The charge contours are shown in the range 0.01–0.14 e au^{-3} with an interval of 0.01 e au^{-3}.

The electronic charge density plots of the Xe adsorbed nanotubes reveal quite weak binding between the Xe and the host nanotube. As an example, we depict the charge density plots on a cross-section of a (10, 10) nanotube containing one Xe on the surface of the tube in figure 7. Here, we depict the excess charge of the Xe-doped tube over the pristine tube. The charge contours are shown in the range 0.01–0.14 e au^{-3} with an interval of 0.01 e au^{-3}.

3.3. Optical absorption

We calculate the optical absorption spectra of the isolated nanotube and the Xe-doped tubes using the absorption coefficient (Hybertson and Needles 1993) by

$$\alpha(\omega) = \frac{4\pi^2 e^2}{ncm^2\omega V_c} \sum_{v,c,\vec{k}} \left| \vec{\varepsilon} \cdot \vec{p}_{cv}(\vec{k}) \right|^2 \delta(E_c - E_v - \hbar\omega), \tag{3}$$

with m and e as the electron mass and charge, c as velocity of light, n the refractive index and V_c the unit cell volume including the empty space. $\vec{\varepsilon}$ denotes an unit electric vector of the incident polarized light. E_c and E_v are the energies of the conduction and the valence states for the wavevector $\vec{k}$. The momentum operator matrix element $\vec{p}_{cv}(\vec{k})$ is given by

$$\vec{p}_{cv}(\vec{k}) = \langle \psi_c, \vec{k} | \vec{p} | \psi_v, \vec{k} \rangle, \tag{4}$$

where ψ_c and ψ_v denote the wavefunctions of the conduction and the valence states, respectively. $\vec{p}$ is the momentum operator.

In the actual calculation, for simplicity, we consider the polarization of light confined in one direction x, y or z. Further, the absorption has been obtained using a broadening of 0.1 eV to avoid the spiky structure arising from our choice of a coarse grid in the BZ to cope with the limited memories of the computer available to us.

The no-phonon optical absorption for the incident electromagnet polarization along the tube axis obtained for the various Xe-tube configurations is compared with the pristine tubes in figures 8–10. In all cases, the absorption normal to the axis of each nanotube is quite small.

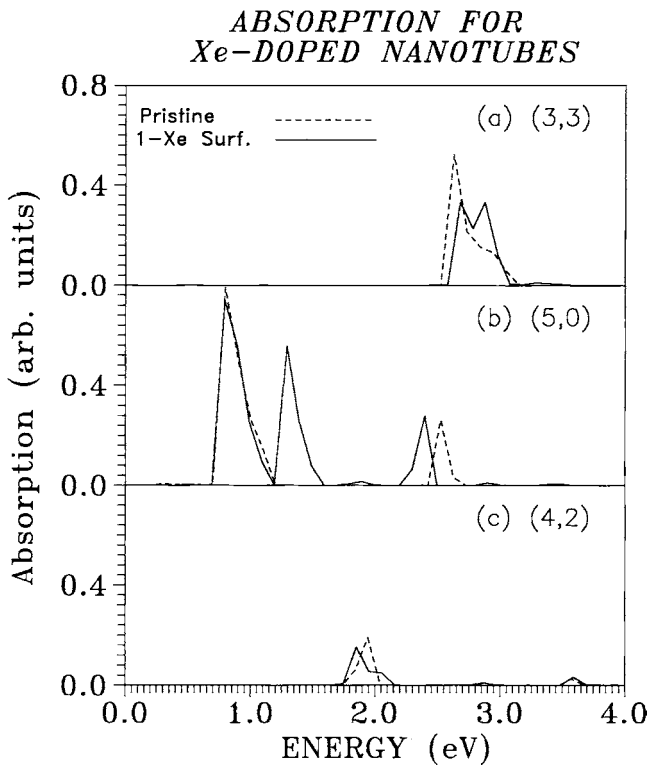

Figure 8. Absorption spectra in the energy range 0–4.0 eV for the (a) (3, 3), (5, 0) and (4, 2) nanotubes, respectively.

(3, 3) nanotube. For the pristine (3, 3) nanotube, the optical absorption along the tube axis is shown in figure 8(a). One observes a strong peak having its low-energy edge at 2.9 eV. The peak is quite close to the experimentally observed peak at 3.1 eV in Lie *et al* (2001) and Liang *et al* (2002) in 4 Å nanotubes. The present value of 2.9 eV is also near to the calculated values of Machon *et al* (2002) and of Liu and Chan (2003), who have obtained a peak at 2.8 eV. Spataru *et al* (2004) have also obtained a peak at 2.83 eV in LDA and have shown that the consideration of the many-body effects including the excitonic contribution will raise the peak to 3.17 eV, which is closer to the experimental value of 3.1 eV.

The transition between the states numbered as 24th and 25th at $k_z = 0$ are forbidden by symmetry considerations. It should be noted that appreciable optical absorption for (3, 3) nanotubes whether pristine or doped with Xe atoms is observed only for the wavevector range $k_z = 0.38$–0.48. Also, the main peak at 2.9 eV arises from the transitions between the doubly-degenerate occupied (23, 24) and the unoccupied (25, 26) states in the wavevector range $k_z = 0.4$–0.48 as shown in figure 3(a). It may be cautioned that the present numbering of states is changed at different values of $k_z > 0.40$ and is totally different from the numbering of states at $k_z = 0$.

1-Xe. For the (3, 3) nanotube having one Xe per unit cell adsorbed on the surface, the peak at 2.9 eV of the undoped tube splits into two peaks (figure 8(a)). For the Xe-doped (3, 3) tube too, as regards to the participation of the states giving rise to absorption, the situation is exactly similar to that of the pristine tube, except in the enhanced numbering of the participating states which are increased by four because of the adsorption of the Xe atoms.

(5, 0) nanotube. The optical absorption for the pristine (5, 0) nanotube shown in figure 8(b) reveals one broad strong peak at 0.9 eV and a weak peak at 2.5 eV. The present peaks are quite near to the experimental ones observed at 1.2, 2.1 and 3.1 eV for the pristine 4 Å carbon tubes in Lie *et al* (2001) and Liang *et al* (2002). Also, the present peaks are quite close to the calculated values of 1.2 and 2.3–2.4 eV by Machon *et al* (2002) and Liu and Chan (2003). Spataru *et al* (2004) have also obtained a peak at 1.13 eV in LDA and have shown that the discrepancy between the LDA value and the experimental value can be explained if one considers also the many-body effects including the excitonic contribution. The experimental peak at 1.2 eV is assigned to the (5, 0) tube. It may be mentioned that the optical absorption arises mainly from the wavevector range $k_z = 0$–0.08 and involves all the 37th to 45th states at different values of k_z. The transitions between the occupied (40, 41) and the unoccupied (42, 43) states are forbidden by symmetry considerations. The peak around 0.9 eV arises from the transition between the doubly-degenerate occupied (38, 39) states and the doubly-degenerate unoccupied (42, 43) states. On the other hand, the peak at 2.5 eV originates from the transitions between the (40, 41) and the (44, 45) states.

1-Xe. For 1-Xe adsorbed on the surface of the (5, 0) nanotube as presented in figure 8(b), the strong peak seen at 0.9 eV in the absorption of the pristine tube is retained. Another strong peak appears at 1.3 eV. Similarly to the pristine tube, a weak peak also appears at 2.4 eV. The participation of the states in the absorption at 0.9 and 1.3 eV is similar to those seen earlier in the pristine (5, 0) tube except for the numbering of the participating states, which are enhanced to the 42, 43 (valence) states and the 46, 47 (conduction) states. For more than 1-Xe atom adsorbed on the (5, 0) nanotube, the absorption is seen to have a similar nature.

(4, 2) nanotube. For the (4, 2) nanotube, we have obtained the optical absorption for one k-point only to have manageable computer time. For the pristine (4, 2) nanotube, the optical absorption is shown in figure 8(c). A peak occurs at 1.95 eV along with two very weak peaks at 2.9 and 3.6 eV. The strong peak at 1.95 eV originates from the transitions between the occupied (107, 108, 111) and the unoccupied (115, 116, 118) states at $k_z = 0.0$.

Our peaks are in good agreement with the measured peak at 2.1 eV for 4 Å carbon tubes in Lie *et al* (2001) and Liang *et al* (2002) and the calculated peaks at 1.9, 2.9–3.0 and 3.6 eV in Machon *et al* (2002) and Liu and Chan (2003).

For 1-Xe atom residing on the surface of the (4, 2) tube, the optical absorption is shown in figure 8(c). Quite similarly to the pristine (4, 2) nanotube, a peak appears at 1.85 eV along with two very weak peaks at 2.9 and 3.6 eV. The strong peak at 1.85 eV arises from the transitions between the occupied (111, 112, 115, 116) and the unoccupied (117, 118, 121, 122) states at $k_z = 0.0$.

(10, 0) nanotube. The optical absorption for the pristine (10, 0) nanotube as shown in figure 9(a) reveals four peaks having edges at 0.9, 2.1, 2.6 and 3.0 eV. The number has doubled as compared to that seen for the (5, 0) tube, and two extra peaks are now seen at 2.0 and 3.1 eV. The present peaks at 0.9 and 2.1 eV are quite near to the experimental peaks observed at 0.95, 1.12, 1.8 and 2.25 eV measured in absorption and emission by O'Connell *et al* (2002) in a mixture of single-walled nanotubes possessing tube diameters in the range 7–11 Å.

It may be mentioned that the peaks at 2.25 and 3.5 eV in the optical absorption have been reported by the present authors (Agrawal *et al* 2003) for the isolated armchair (6, 6) nanotube of diameter of 8.19 Å. The peak at 2.25 eV is in excellent agreement with the measured data of O'Connell *et al* (2002).

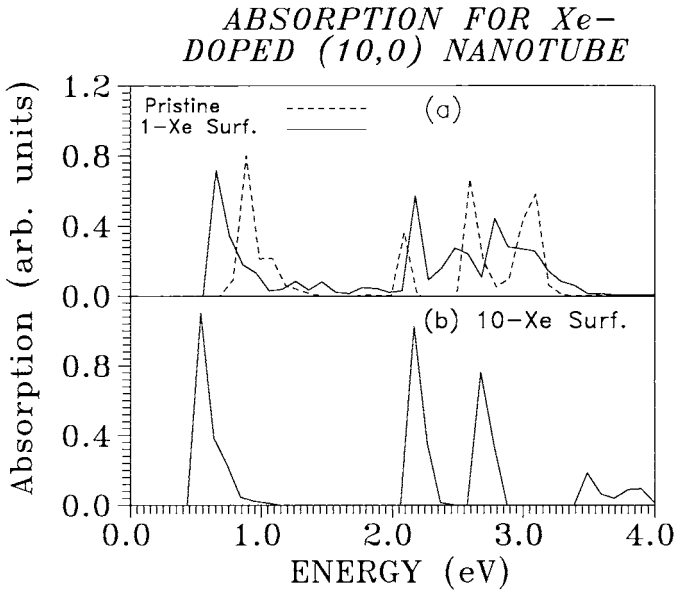

Figure 9. Absorption spectra in the energy range 0–4.0 eV for a (10, 0) nanotube: (a) pristine and 1-Xe atom on surface site, (b) 10-Xe atoms on surface sites.

The optical absorption arises mainly from the wavevector range of $k_z = 0$–0.08 and involves all the 73rd to 89th states at different values of k_z. The peak around 0.9 eV arises from the transitions between the doubly-degenerate occupied (79, 80) states and the doubly-degenerate unoccupied (81, 82) states. On the other hand, the peak at 2.1 eV originates from the transitions between the occupied (77, 78) and the unoccupied (88, 89) states. The other high-energy peak at 2.6 eV corresponds to the transitions between the filled (75, 76) states and the vacant (86, 87) states, whereas the peak at 3.0 eV is generated by the occupied (73, 74) and the unoccupied (83–85) states.

1-Xe. For 1-Xe atom adsorbed on the surface mid-bond site on the (10, 0) nanotube, the absorption presented in figure 9(b) again reveals four peaks but at slightly altered locations. Again, the absorption is the same for all types of sites. The peaks appear at 0.65, 2.2, 2.5 and 2.8 eV. As compared with the peaks seen in the pristine tube, the lowest energy peak has shifted to the lower energy side by 0.25 eV (to 0.65 eV). The high-energy peak at 3.0 eV seen for the pristine tube is now quite weak.

The participation of the states in the absorption at 0.65 eV is exactly similar to those seen earlier in the pristine (5, 0) tube except for the numbering of the participating states which are enhanced by four. The participating states are the (83, 84) valence states and the conduction (85, 86) states. Similar arguments are valid for the other peaks regarding the participation of the states in the optical transitions.

For 10-Xe atoms adsorbed on the surface mid-hexagonal sites on the (10, 0) nanotube, the absorption presented in figure 9(b) reveals only three strong peaks at 0.65, 2.2, and 2.7 eV.

(10, 10) nanotubes. For the pristine (10, 10) nanotube, the optical absorption along the tube axis is shown in figure 10(a). One observes weak absorption near 2.0 eV and appreciable absorption in the energy range 2.7–4.0 eV including three strong peaks at 2.8, 3.5 and 3.7 eV. Two peaks are quite close to the two out of the four experimentally observed peaks at 0.7, 1.3,

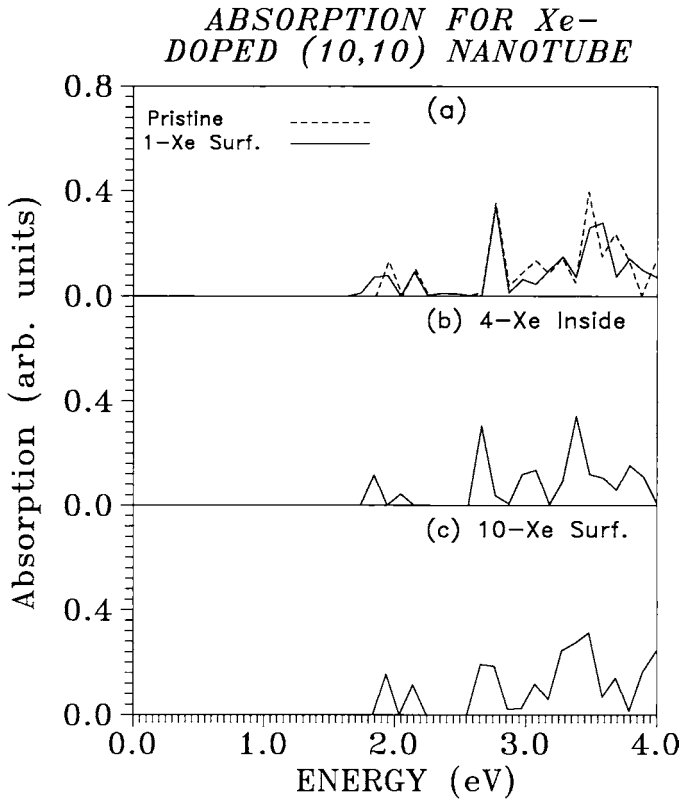

Figure 10. Absorption spectra in the energy range 0–4.0 eV for a (10, 10) nanotube: (a) pristine and 1-Xe atom on surface site, (b) 4-Xe atoms inside and (c) 10-Xe atoms on surface sites.

1.9 and 2.6 eV in the mixture of single-walled nanotubes of 14 Å diameter in Hwang *et al* (2000). Kazaoui *et al* (2000) have also observed peaks at 1.2, 1.8 and 2.4 eV in a mixture of isolated and bundles of tubes having diameters in the range 12–16 Å. Variation in the peak positions with the tube diameter in the range 9–14 Å in bundles of mixed tubes have been reported by Liu *et al* (2002). In the experiments, a peak at 0.7 eV has been reported which is not seen in our calculation for the pristine (10, 10) nanotube. This low-energy peak may arise from the same diameter tubes of other chiralities present in the measured sample. The predicted peak structure near 3.6 eV has not been reported as yet to the knowledge of the authors.

The transition between the states numbered as 80th and 81st at $k_z = 0$ are forbidden by symmetry considerations. As noted for the armchair (3, 3) tube, here too appreciable optical absorption for the nanotubes whether pristine or doped with the Xe atom is observed only for the wavevector range $k_z = 0.38$–0.44. The weak peak at 2.0 eV arises from the transitions between the doubly-degenerate occupied (78, 79) and the unoccupied (82, 83) states as shown in figure 6(a). The other peak at 2.8 eV arises from the combinations of the occupied (76, 77) states and the unoccupied (84, 85) states. The highest energy peaks at 3.5 and 3.7 eV originate from combinations of the valence (74–79) and the conduction (83–91) states.

1-Xe. For the (10, 10) nanotube having one Xe per unit cell whether inside or outside the tube, the peak structure (figures 10(a) and (b)) is quite similar to that of the pristine tube

except for some minor differences. For the 1-Xe-doped (10, 10) nanotube too, as regards the participation of the states giving rise to absorption, the situation is exactly similar to that of the pristine tube except in the enhanced numbering of the participating states, which are increased by four because of the adsorption of the Xe atom. For the endohedral adsorption, almost all the peaks are shifted to the low-energy side by about 0.2 eV.

10-Xe. For the (10, 10) nanotube having ten Xe atoms per unit cell outside the tube, the optical absorption is quite similar to that of the pristine tube.

4. Conclusions

The most favoured tubes for Xe atom adsorption are armchair (n, n) tubes, and Xe adsorption on the surfaces on zigzag $(n, 0)$ and chiral (m, n) tubes may not be observed. The endohedral adsorption in the comparatively large-diameter (10, 0) tube is strong because of the large contribution of the vdW energy. Regarding the binding of the Xe atom on the different types of the surface sites, we observe that the binding is strongest on the mid-hexagonal site on all the achiral nanotubes. For the chiral (4, 2) tube, the preferred Xe-site is above the mid-bond site of the C–C bond.

Quite small changes in the diameters of the nanotubes are induced by the adsorption of the Xe atoms. Negligible buckling is observed for the endohedral adsorption in the large-diameter tubes. For the exohedral adsorption, one observes site-dependent buckling. The buckling is appreciable for the achiral (5, 0), the chiral (4, 2) and the large-diameter (10, 0) tube. There is variation in the minimum Xe–C separation with the site as well as with the adsorbed concentration of Xe atoms. This C–Xe separation is large for the endohedral adsorption.

The saturation concentration of the Xe atoms adsorbed on the surface of the (3, 3) and (10, 10) tubes is estimated to be 25 and 2.5%, respectively. On the other hand, the maximum endohedral adsorption in the (10, 0) and (10, 10) tubes is 2.5 and 10.0%, respectively.

In view of the idealized nature of the present calculation and the uncertainty in the measurements, the presently calculated values for the binding energy of 0.315 eV and the saturation endohedral Xe adsorbate concentration of 10% are in reasonable agreement with the measured data available for (10, 10) nanotubes (Weber *et al* 2000, Talapatra *et al* 2000, Zambano *et al* 2001, Kuznetsova *et al* 2000, Simonyan *et al* 2001).

The electronic structure of the pristine tube is changed by the adsorption of the Xe atom on the surface of the tube because of the breaking of the symmetry of the host lattice, except for the chiral (4, 2) tube which has practically no symmetry. The adsorption incurs splitting in the states in the whole energy range especially in the large-curvature 4 Å tubes. In the armchair (n, n) tubes, the adsorption of the Xe atom raises one valence state up to E_F and converts it into a mixed C(p)–Xe(p) state. Additional electrical conductive channels are generated by the Xe adsorption. The band gap of semiconducting achiral zigzag nanotube is reduced by the adsorption of the Xe atom. On the other hand, the bandgap of a chiral semiconducting tube is enhanced by the adsorption of the Xe atom.

In the optical absorption for one Xe atom on the small-diameter 4 Å armchair (3, 3) tube, the peak of the pristine tube splits into two peaks. On the other hand, in the optical absorption of the (5, 0) tube, the adsorption of one Xe atom on the surface does not alter the peak structure seen for the pristine tube except for the appearance of an extra strong peak at 1.3 eV. For the chiral (4, 2) tube, the adsorption of the Xe atom does not change the peak structure of the optical absorption of the pristine tube.

Some of the calculated peaks in the optical absorption of the pristine (10, 0) tube have been observed in experiments. For 1-Xe atom adsorbed on the surface mid-hexagonal site on

the (10, 0) nanotube, the absorption again reveals four peaks similar to the pristine tube but at slightly changed locations. However, for a tube of 10-Xe atoms around the (10, 0) tube, the number of peaks reduces to three.

Again, some of the calculated peaks in the optical absorption in the pristine (10, 10) nanotube have been detected in a number of experimental measurements. For the large-diameter (10, 10) nanotube again, the peak structure in the optical absorption of the pristine tube remains practically unaffected by the adsorption of the Xe atoms.

Acknowledgments

The authors express thanks to the University Grants Commissions and Defence Research Development Organization, New Delhi for financial assistance and to Dr P S Yadav for providing us with the computation facilities.

References

Agrawal B K, Agrawal S and Srivastava R 2003 *J. Phys.: Condens. Matter* **15** 6931
Agrawal B K, Agrawal S, Srivastava R and Singh S 2004 *Phys. Rev.* B **70** 075403
Ajayan P M, Ebbesen T W, Ichihashi T, Ijima S, Tanigaki K and Hiura H 1993 *Nature* **362** 522
Akai Y and Saito S 2003 *Japan. J. Appl. Phys.* **42** 640
Becke A D 1988 *Phys. Rev.* A **38** 3098
Collins P G, Bradley K, Ishigami M and Zettl A 2000 *Science* **287** 1801
Dag S, Gulseren O, Yildirim T and Ciraci S 2003 *Phys. Rev.* B **67** 165424
Dresslhaus M S, Williams K A and Eklund P C 1999 *Mater. Res. Soc. Bull.* **24** 45 (for a review of earlier work)
Durgun E, Dag S, Bagei V M K, Gulseren O, Yildirim T and Ciraci S 2003 *Phys. Rev.* B **67** 201401 and the references therein
Fuchs M and Scheffler M 1999 *Comput. Phys. Commun.* **119** 67
Giannozzi P, Car R and Scoles G 2002 *J. Chem. Phys.* **118** 1003
Goedecker S 1997 *SIAM J. Sci. Comput.* **18** 1605
Gonze X 1996 *Phys. Rev.* B **54** 4383
Halgrem T A 1992 *J. Am. Chem. Soc.* **114** 7827
Hirscher M, Becher M, Haluska M, Quintel A, Skakalova V, Choi Y M, Dettlaff-Weglikowska U, Roth S, Stepanek I, Bernier P, Leonhardt A and Fink J 2002 *J. Alloys Compounds* **330** 654
Hwang H, Gommans H H, Ugawa A, Tashiro H, Haggenmueller R, Winey K I, Fischer J E, Tanner D B and Rinzler A G 2000 *Phys. Rev.* B **62** R13310
Hybertson M S and Needles M 1993 *Phys. Rev.* B **48** 4608
Kazaoui S, Minami N, Yamawaki H, Aoki K, Kataura H and Achiba Y 2000 *Phys. Rev.* B **62** 1643
Kleinhammes A, Mao S H, Yang X J, Tang X P, Shimoda H, Lu J P, Zhou O and Wu Y 2003 *Phys. Rev.* B **68** 075418
Kleinman L and Bylander D M 1982 *Phys. Rev. Lett.* **48** 1425
Kong J, Franklin N R, Zhou C W, Chapline M G, Peng S, Cho K J and Dai H J 2000 *Science* **287** 622
Kuznetsova A, Yates J T Jr, Liu J and Smalley R E 2000 *J. Chem. Phys.* **112** 9590
Lee C, Yang W and Parr R G 1988 *Phys. Rev.* B **37** 785
Liang W, Chen G, Li Z and Tang Z K 2002 *Appl. Phys. Lett.* **80** 3415
Lie Z M, Tang Z K, Liu H J, Wang N, Chan C T, Saito R, Okada S, Li G D, Chen J S, Nagasawa N and Tsuda S 2001 *Phys. Rev. Lett.* **87** 127401
Liu H J and Chan C T 2003 *Solid State Commun.* **125** 77
Liu X, Pichler T, Knupfer M, Golden M S, Fick J, Kataura H and Achiba Y 2002 *Phys. Rev.* B **66** 045411
Machon M, Reich W, Thomson C, Sanchez-Portal D and Ordejon P 2002 *Phys. Rev.* B **66** 155410
Mackie E B, Wolfson R A, Arnold L M, Lafdi K and Migone A D 1997 *Langmuir* **13** 7197
O'Connell M J, Bachilo S M, Huffman C B, Moore V C, Strano M S, Haroz E H, Rialon K L, Boul P J, Noon W H, Kittrell C, Ma J, Hauge R H, Weisman R B and Smalley R E 2002 *Science* **297** 593
Odom T W, Huang J L, Kim P and Lieber C M 1998 *Nature* **391** 62
Payne M C 1992 *Rev. Mod. Phys.* **64** 1045
Perdew J P, Burke K and Ernzerhof M 1996 *Phys. Rev. Lett.* **77** 3865
Saito Y, Nishiyama T, Kato T, Kondo S, Tanaka T, Yotani J and Uemura S 2002 *Mol. Cryst. Liq. Cryst.* **387** 303

Schlapbach M and Zuttel M 2001 *Nature* **414** 353
Shi W and Johnson J K 2003 *Phys. Rev. Lett.* **91** 015504
Shim M, Kam N W S, Chen R J, Li Y M and Dai H J 2002 *Nano Lett.* **2** 285
Siber A 2003 *Phys. Rev.* B **68** 033406
Simonyan V V, Jonhnson J K, Kuznetsova A and Yates J T Jr 2001 *J. Chem. Phys.* **114** 4180
Skoulidas A I, Ackerman D M, Johnson J K and Shool D S 2002 *Phys. Rev. Lett.* **89** 185901
Spataru C D, Beigi S I, Benedict L X and Louie S G 2004 *Phys. Rev. Lett.* **92** 77402
Stan G, Bojan M J, Curtarolo S, Gatica S M and Cole M W 2000 *Phys. Rev.* B **62** 2173
Sumanasekera G U, Adu C K W, Fang S and Eklund P C 2000 *Phys. Rev. Lett.* **85** 1096
Talapatra S, Zambano A J, Weber S E and Migone A D 2000 *Phys. Rev. Lett.* **85** 138
Troullier N and Martins J L 1991 *Phys. Rev.* B **43** 1993
Tsang S C, Chen Y K, Harris P J F and Green M L H 1994 *Nature* **372** 159
Weber S E, Talapatra S and Migone A D 2000 *Phys. Rev.* B **61** 13150
Wildoer J W G, Vnema L C, Rinzler A G, Smalley R E and Dekker C 1998 *Nature* **391** 59
Zambano A J, Talapatra S and Migone A D 2001 *Phys. Rev.* B **64** 075415
Zhao J, Buldum A, Han J and Lu J P 2002 *Nanotechnology* **13** 195